Available online at www.sciencedirect.com
SCIENCE DIRECT
Microporous and Mesoporous Materials 94 (2006) 277–282
MICROPOROUS AND MESOPOROUS MATERIALS
www.elsevier.com/locate/micromeso

# Phosphating alumina: A way to tailor its surface properties

Jaime S. Valente [a,*], Sofía Falcón [a], Enrique Lima [b,c], Marco A. Vera [b], Pedro Bosch [c], Esteban López-Salinas [a]

[a] Instituto Mexicano del Petróleo, Eje Central L. Cárdenas 152, AP 14-805, 07730 México, DF, Mexico
[b] Universidad Autónoma Metropolitana, Iztapalapa, Av. San Rafael Atlixco No. 186, AP 55-532, 09340 México, DF, Mexico
[c] Instituto de Investigaciones en Materiales, UNAM, Circuito Exterior, AP 70-360, 04510 México, DF, Mexico

Received 13 December 2005; received in revised form 15 February 2006; accepted 17 February 2006
Available online 30 May 2006

**Abstract**

Phosphated alumina with new surface properties was prepared by sol–gel synthesis. Aluminum coordinately unsaturated sites (CUS) were promoted and tuned through phosphate addition. Two phosphate species on alumina were disclosed by $^{31}P$ MAS NMR spectroscopy. The population of aluminum CUS was related to the amount of phosphorus incorporated into the alumina network. The relative amount of phosphorus species was controlled by the alumina gel's aging time. X-ray diffraction, performed on calcined solids, identified a microcrystalline structure of γ-alumina. Phosphated aluminas showed both high surface areas (364–394 $m^2/g$) and total pore volume (1.0–1.2 $cm^3/g$), even after calcining at 550 °C.


*Keywords:* Catalysts; MAS NMR spectroscopy; X-ray diffraction; Sol–gel preparation; Phosphated alumina

## 1. Introduction

Transition aluminas are conventionally produced through precipitation, drying, and thermal dehydration of aluminum oxy-hydroxides. These oxides have been extensively used as absorbents, ceramics, composite materials, and as catalysts or catalyst supports in several chemical processes [1–3].

The catalytic properties of aluminas depend on their chemical structure and texture. Acidity plays an important role on the activity and selectivity of catalysts, as they are intimately related to the amount, strength, and nature of acid sites [4–7]. Therefore, the ability to control support acidity proves to be a crucial parameter. In industry, tuning the type and strength of acid sites on aluminas is highly recommended. As a huge infrastructure to produce alumina has already been installed, alumina is always preferred over other metal oxides. Since the creation of $Al^{IV}$ and $Al^{V}$ species aluminum coordinately unsaturated sites (CUS) must be accompanied by a redistribution of the charge on the aluminum and oxygen atoms, the acidity of aluminas and aluminosilicates catalysts is related to aluminum coordination and to the chemical nature of its neighbors. Therefore, the CUS amount, vicinity, and accessibility could be the key to controlling their catalytic properties [4–7].

Alumina is conventionally dehydrated during preparation producing CUS which, in turn, create Lewis acidity. However, control over the acid site types and number is highly desirable because Brönsted acid sites are necessary in order to achieve skeletal rearrangements. Several strategies to obtain the required acid features have been proposed. In one instance, $H_3PO_4$ or $H_2SO_4$ supported on $Al_2O_3$, $ZrO_2$, and $SiO_2$–$Al_2O_3$ exhibit high activities and selectivities for different organic reactions [8–11]. Despite the fact that several studies have been done on phosphated aluminas their surface is not yet fully understood [11–14]. Furthermore, such knowledge should lead to the control of the surface features, and thus, of the catalytic reaction.

* Corresponding author. Tel.: +52 55 9175 8444.
*E-mail address:* jsanchez@imp.mx (J.S. Valente).

1387-1811/$ - see front matter © 2006 Published by Elsevier Inc.
doi:10.1016/j.micromeso.2006.02.018

Among the synthesis methods that can be used to prepare aluminas, the sol–gel method provides an attractive and convenient route by enabling an accurate control over the structural and textural properties such as high specific surface area, uniform pore size distribution, and high purity.

In sol–gel methods, aging represents the time between the formation of a gel and the removal of solvent. As long as the pore liquid remains in the matrix, a gel is not static and therefore can undergo many transformations [15,16]. For alkoxide derived gels, condensation between surface functional groups continues to occur after the gel point. This process can actually be desirable because it leads to a more cross-linked network that is mechanically stronger and easier to handle; however, extensive condensation causes the gel to shrink. Aging is often an overlooked step in the sol–gel preparation of catalytic materials. The work of Smith et al., who developed an in situ NMR technique to follow the aging process, demonstrates the importance of this parameter [17].

In this work, sol–gel phosphated aluminas aged for several days are studied. The effect of the aging time on phosphated aluminas was studied to unveil the evolution of the type and relative amount of phosphate and aluminum species in the bulk and on the surface.

## 2. Experimental

### 2.1. Synthesis

Aluminum tri-sec-butoxide (ATB) (97%) was dissolved and refluxed at 80 °C in absolute anhydrous ethyl alcohol (EtOH) for 1 h. Phosphoric acid (3 N), used as a hydrolysis catalyst, was slowly added into the solution while stirring and refluxing for 1 h. The system was then cooled down to room temperature, allowing the hydrolysis to complete and form a gel. The molar ratios of reactants were EtOH:ATB = 60:1, $H_3PO_4$:ATB = 0.03:1, and $H_2O$:ATB = 1:1. The gel was placed in a glass vessel and aged for several days. The samples were labeled as APE1, APE10, APE20, or APE30, according to the number of days aged. Thereafter, the product was dried overnight at 100 °C. Dried solids were calcined in the air from room temperature up to 550 °C at 4 °C/min for 4 h.

### 2.2. Characterization techniques

#### 2.2.1. Phosphorus content

The amount of phosphorus in the solid phosphated aluminas was measured by means of inductively coupled plasma (ICP), using a Perkin–Elmer OPTIMA 3200DV spectrometer, where 0.1–0.2 g of alumina samples were digested with nitric acid. After this, a portion of the sample was transferred into the nebulization chamber through a peristaltic pump at 1 $cm^3$/min using argon as the carrier gas.

#### 2.2.2. Textural properties

All textural properties on calcined materials were determined using Quantachrom Autosorb-1 equipment. Specific surface area was calculated with the Brunauer–Emmet–Teller (BET) equation from $N_2$ adsorption at −196 °C. Pore size distribution was obtained by the Barrett–Joyner–Halenda (BJH) method in the desorption stage.

#### 2.2.3. Thermal analyses

Phase transformation as a function of temperature was examined by differential thermal analysis using a Perkin–Elmer DTA-1700, with inflowing air at 20 $cm^3$/min, and a heating rate of 10 °C/min.

#### 2.2.4. X-ray powder diffraction

Diffraction patterns were obtained via a Siemens D500 diffractometer coupled with a molybdenum anode X-ray tube (Kα radiation). Compounds were identified using the JCPDS files.

#### 2.2.5. NMR measurements

The $^{27}Al$ and $^{31}P$ NMR experiments were recorded on a Bruker ASX 300 spectrometer operating at resonance frequencies of 78.2 MHz for $^{27}Al$ and 121.4 MHz for $^{31}P$ MAS NMR spectroscopy. All MAS NMR spectra were recorded after single π/2 excitation with repetition times of 500 ms for $^{27}Al$ and 20 s for $^{31}P$. The samples were spun at 10 kHz for $^{27}Al$ and 5 kHz for $^{31}P$ MAS NMR, and the chemical shifts were referenced to 1 N aqueous solution of $AlCl_3$ for $^{27}Al$ and $H_3PO_4$ for $^{31}P$. To disclose the aluminum location, cross-polarization (CP) MAS NMR experiments were also done, since this technique is sensitive and reliable for determining aluminum species on the surface. $^1H$–$^{27}Al$ CP-experiments restrict the NMR signal to aluminum nuclei that are near protons, i.e. at or near the surface, as is the case in OH groups. The CP contact time was 3 ms for $^{27}Al$.

## 3. Results and discussion

As shown in Table 1, phosphated aluminas showed similar phosphorus contents, ranging from 0.49 to 0.58 wt.%, regardless of aging time. These values are very close to the nominal one.

Specific surface area (SSA) of phosphated aluminas decreased with aging time, as indicated in Table 2. Crystallite size in aluminas increases with aging time when keeping all other synthesis variables constant. It is well known that

Table 1
Phosphorus content in phosphated aluminas

| Sample | Aging time (day) | Phosphorus (wt.%) |
|---|---|---|
| APE1 | 1 | 0.55 |
| APE10 | 10 | 0.53 |
| APE20 | 20 | 0.49 |
| APE30 | 30 | 0.58 |

Table 2
Specific surface area, pore volume, and average pore size of phosphated aluminas

| Sample[a] | BET surface area ($m^2/g$) | Pore volume ($cm^3/g$) | Average pore size (Å) |
|---|---|---|---|
| APE1 | 394 | 1.01 | 96 |
| APE10 | 389 | 1.02 | 98 |
| APE20 | 378 | 1.20 | 119 |
| APE30 | 364 | 1.19 | 123 |

[a] All samples were calcined at 550 °C for 4 h.

SSA varies as a function of particle size, shape, and porosity. The relationship between SSA, the total pore volume $V_p$, and the average pore radius $r_p$ is given by

$$\mathrm{SSA} = fV_p/r_p$$

where $f$ depends on the pore's geometry, such as whether they are cylindrical, spherical, or formed by parallel plates. Assuming $f$ to be constant for all samples, since the shape of adsorption–desorption hysteresis loops is similar among them (see Fig. 1), and that $V_p$ and average pore size increased with time, especially after 20 and 30 days, then the SSA decrease is more a consequence of the pore size increase than of the pore volume. That is because pore size increased 28% and pore volume increased 18%, relative to the 1-day sample. Aluminas prepared by a combination of a sol–gel method, using HCl as a hydrolysis catalyst, and hydrothermal treatment, showed a drastic SSA decrease when aging the gel for up to 15 days [18]. Total pore volume in phosphated aluminas was considerably high (1.01–1.20 $cm^3/g$), especially in the samples aged 20 and 30 days. Accordingly, γ-aluminas with high total pore volumes (1.0–1.33 $cm^3/g$) can be obtained by sol–gel methods even after calcining at temperatures between 550 °C and 700 °C [18,19]. Recently, Bokhimi et al. have reported that alumina nanocapsules obtained by a sol–gel method using $H_2SO_4$ as a hydrolysis catalyst and 20 days of aging showed a total pore volume of 1.33 $cm^3/g$ after calcining at 700 °C [20]. The importance of high pore volume catalysts or catalyst supports is reflected in the total volume of the final reactor or vessel which will be smaller, and thus economic, in terms of catalyst and/or support masses.

According to IUPAC classification and Fig. 1(a)–(d), all isotherms are of type IV and hysteresis loops are type H1, typically found on solids with homogeneous pore size distribution and uniform particle size. Pore size distributions of phosphated aluminas (insets in Fig. 1(a)–(d)) showed that, with the exception of the average pore size, aging time did not considerably affect their relative distributions

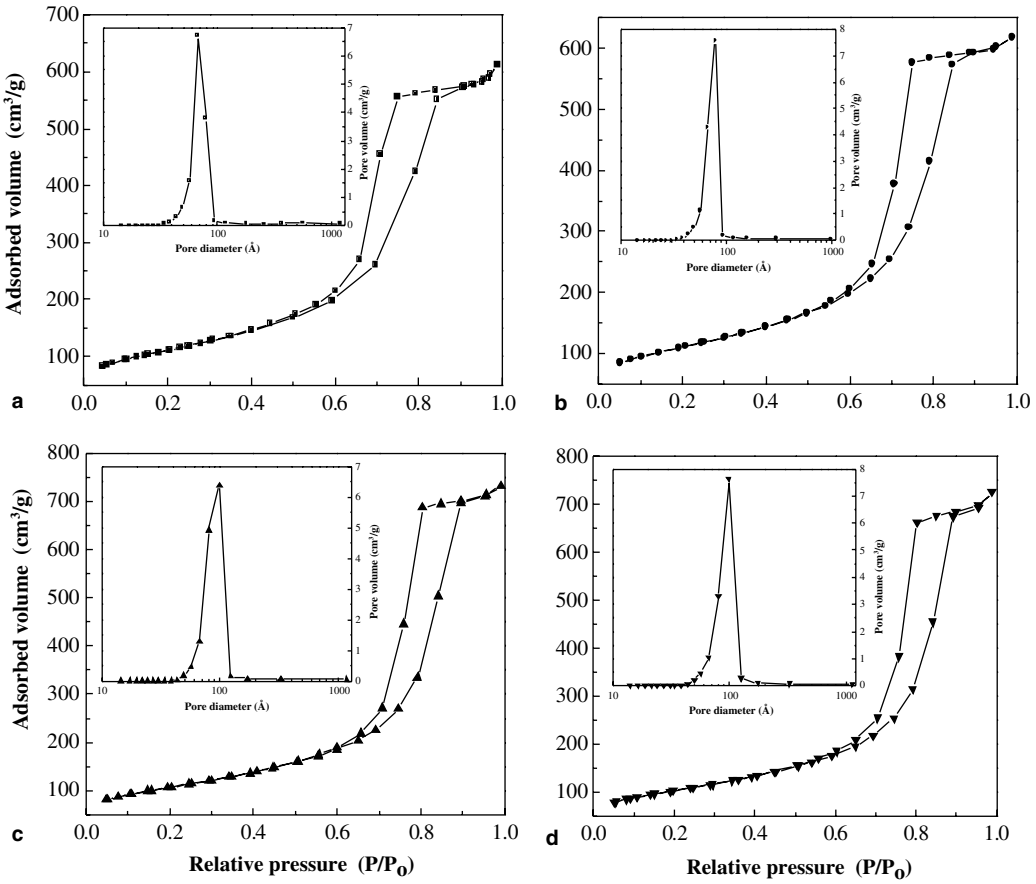


Fig. 1. Adsorption–desorption isotherms of phosphated aluminas; the inset shows pore size distributions: (a) APE1, (b) APE10, (c) APE20, (d) APE30. All samples were calcined at 550 °C.

(see Table 2). It is worthwhile to mention that pore size distributions in all phosphated aluminas were very narrow and were not affected by aging time.

DTA patterns of phosphated aluminas are shown in Fig. 2. In general, phosphated aluminas aged 1-day showed three main thermal events: (i) an endothermic peak at ≈120 °C, (ii) an exothermic peak at ≈270 °C, and (iii) an endothermic peak at ≈310 °C. The first endothermic peak probably corresponds to residual ethanol and/or water adsorbed in the xerogel; the second one, being exothermic, may be ascribed to burn out of residual alkoxy groups; and the third one arises from the dehydroxylation of alumina crystallites. The number of hydroxyl groups in sol–gel aluminas, which have very small crystallite sizes, can be tuned by choosing temperature, aging time, and/or hydrothermal methods [21]. In contrast, DTA patterns of 10-, 20- and 30-day aged aluminas, which are very similar amongst themselves, differed to that of the 1-day aged alumina in that: (i) the exothermic peak appeared at ≈310 °C, and (ii) the second endothermic peak shifted to ≈420 °C. The second endothermic peak in particular is not only shifted, but its broad shape indicates a non-uniform dehydroxylation process, both differences in comparison with those of the 1-day aged sample. This behavior can be rationalized in terms of two effects: (i) population of hydroxyl groups on the surface of the crystallites and (ii) location of phosphate groups. That is, aluminas with a short aging time have a greater number of hydroxyl groups than longer aging aluminas [21]. Additionally, and as will be demonstrated in the NMR section below, phosphate groups in 1-day aluminas are located mainly in the bulk of the crystallite, while a long aging time causes phosphate groups to migrate to the surface, which eventually delays and/or hinders the dehydroxylation process.

The X-ray diffraction patterns (Fig. 3) show that the obtained compounds have the microcrystalline structure $\gamma$-$Al_2O_3$. No evidence of crystalline phosphorus compounds was observed. Nonetheless, note that the phosphorus content is well beyond the XRD detection limits; in fact, a compound can be observed if the amount is higher than 3 wt.% and crystals are larger than 30 Å. Hence, phosphorus species must be highly dispersed in the alumina matrix.

The $^{27}$Al MAS NMR spectra of calcined samples is shown in Fig. 4, where three resonance peaks are observed at ≈0, 30 and 60 ppm, and may be assigned to octahedral

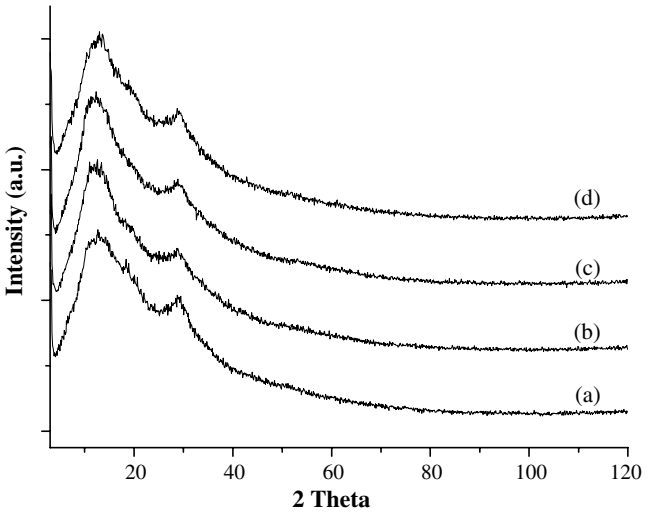


Fig. 3. X-ray diffraction patterns of phosphated aluminas after calcination of gels aged for (a) 1, (b) 10, (c) 20, and (d) 30 days.

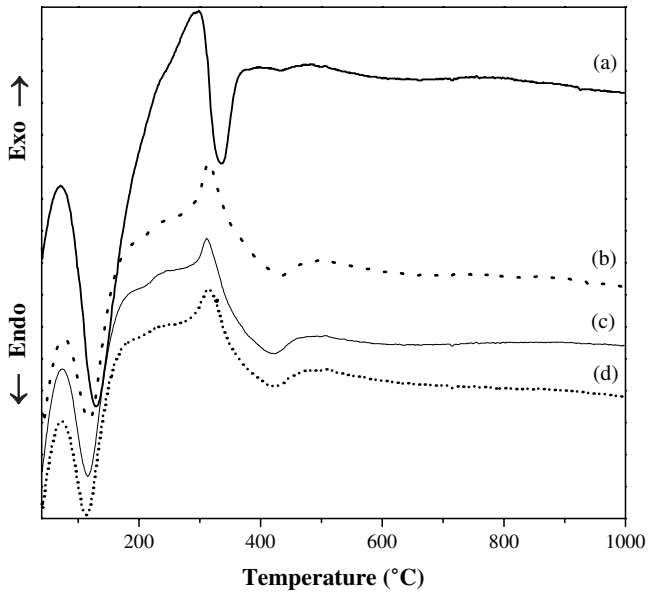


Fig. 2. Differential thermal patterns of fresh phosphated aluminas: (a) APE1, (b) APE10, (c) APE20, and (d) APE30.

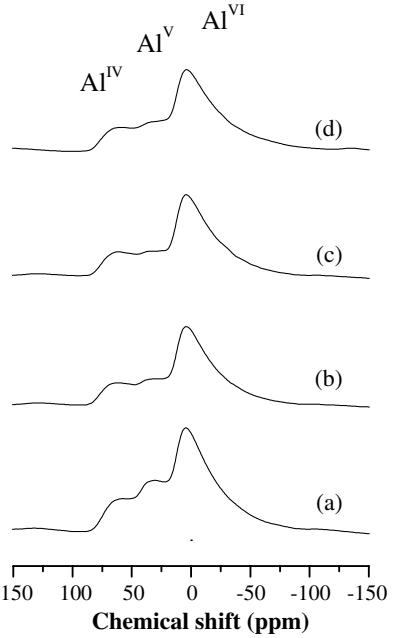


Fig. 4. $^{27}$Al MAS NMR of calcined samples: (a) APE1, (b) APE10, (c) APE20, and (d) APE30.

Table 3
Relative population of Al species from deconvoluted $^{27}$Al MAS NMR spectra

| Sample[a] | Relative distribution (%) | | |
|---|---|---|---|
| | Tetrahedral Al ($\delta = 60$ ppm) | Pentagonal Al ($\delta = 30$ ppm) | Octahedral Al ($\delta = 0$ ppm) |
| APE1 | 12 | 16 | 72 |
| APE10 | 13 | 8 | 79 |
| APE20 | 12 | 5 | 83 |
| APE30 | 13 | 5 | 82 |

[a] All samples were calcined at 550 °C for 4 h.

($Al^{VI}$), pentagonal ($Al^{V}$), and tetrahedral ($Al^{IV}$) aluminum [22,23].

The pentagonal aluminum species decrease as aging time increases (see Fig. 4 and Table 3). In the same manner, the relative number of octahedral sites increases over time from 72% to 82% showing a progressive aggregation of structural elements.

According to Morris and Ellis, by applying $^{1}$H–$^{27}$Al CP NMR it is possible to estimate the relative variation, if any, in the population of Al-species located near the surface or in the bulk [24]. In other words, the Al-species located near the surface will increase their signals, in comparison with those of the original $^{27}$Al MAS NMR spectrum, because protons are mostly located on the surface and will polarize the Al-species located therein. Following the approach of Morris and Ellis, 1-day aged APE1 was selected for the $^{1}$H–$^{27}$Al CP NMR in order to obtain an estimate on bulk and near-surface Al-species variations in populations. The tetrahedral, pentagonal, and octahedral aluminum species resonances were present in the $^{1}$H–$^{27}$Al CP NMR spectra (spectra not shown), indicating that the three types of Al-species are located near the surface. However, they were not present in the same proportion as in the bulk. In fact, as the octahedral peak decreased, an increase in the relative intensities of the tetrahedral and pentagonal peaks was observed, pointing out that the tetra and penta-coordinated aluminum species, i.e. coordinately unsaturated sites (CUS), were present predominantly on the surface. Morris and Ellis have shown that the contribution of the Alumina's interstitial sites to the $^{1}$H–$^{27}$Al CP signal is small when compared to the CP signal resulting from the surface [24]. The aluminum's CUS should have been created during the cross-linking reactions involved in the condensation process of the octahedral units, where phosphorus species form Al–O–P links as in aluminophosphate compounds.

Fig. 5 shows two resonance peaks at −5 and −22 ppm in the $^{31}$P MAS NMR spectra obtained in 1- and 30-day aged phosphated alumina samples. The peak at the weakest field (−5 ppm) is attributed to phosphate groups and the peak at the strongest field (−22 ppm) can be attributed to tetrahedral species $Al(OP)_4$ or $P(OAl)_4$, such as those present in aluminophosphate compounds [25,26].

In the sample aged for 20 days, where a rearrangement of the aluminophosphate species occurs, the relative amount of $PO_4$ increases from 33.9 to 59.0 (see Table 4). Samples aged 30 days showed no indication of any further reordering of phosphate species. Therefore, phosphate groups stay anchored on the surface of the 30-day aged sample. Thus, in gels aged for short periods of time, phosphorus creates mainly $P(OAl)_4$ units. The inclusion of phosphorus in the alumina network causes the displacement of octahedral aluminum to the surface of alumina as pentagonal aluminum. Therefore, the relative amount of phosphorus species in the alumina network and on the alumina surface can be easily tuned by controlling the aging time (see Fig. 6), and most probably by changing the phosphorus load.

Although the formation of CUS sites has been outlined in many works, and the aluminum species have been characterized as transition aluminas, only a few successful examples of tuning their density distribution and stability, beginning at the synthesis step, are known [7,27]. We have found that, with the synthesis method presented in this work, aluminas with new and controllable surface properties may be obtained. As far as we know, there are no previous reports on phosphated alumina synthesis with similar features.

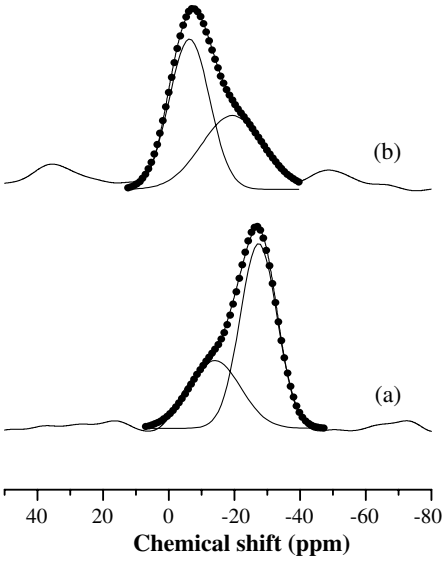


Fig. 5. $^{31}$P MAS NMR spectra of (a) APE1 and (b) APE30 samples. The solid lines correspond to each individual contribution and their sum. The pointed lines correspond to the experimental spectrum.

Table 4
Relative population of phosphorus species from deconvoluted $^{31}$P MAS NMR spectra

| Sample | Distribution (%) | |
|---|---|---|
| | $PO_4$ ($\delta = -5$ ppm) | P–$(OAl)_4$ ($\delta = -22$ ppm) |
| APE1 | 33.9 | 66.1 |
| APE10 | 47.3 | 52.7 |
| APE20 | 58.9 | 41.1 |
| APE30 | 58.0 | 42.0 |

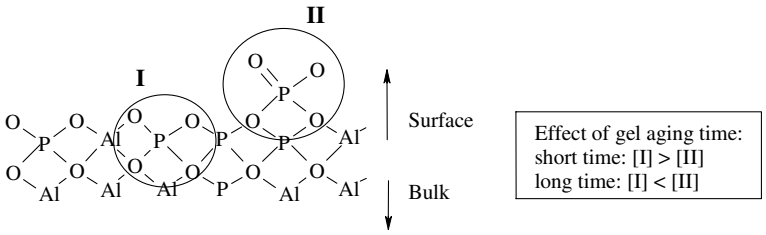


Fig. 6. Phosphorus species model generated in phosphated aluminas prepared by sol–gel procedure.

## 4. Conclusions

In summary, our procedure to obtain sol–gel phosphated aluminas offers a twofold benefit: (1) pentacoordinated aluminum species can be promoted through phosphorus addition, and (2) phosphate groups may be selectively located on the bulk or on the surface of alumina crystallites by controlling aging time. Additionally, phosphated aluminas with both high surface area (364–394 $m^2/g$) and total pore volume (1.0–1.2 $cm^3/g$), even after calcining at 550 °C, can be obtained. Concomitantly, aging time can be used to adjust the average pore size from 96 Å to 123 Å.

## Acknowledgments

This work was supported financially by the IMP, project D.00355. Mr. Jaime F. Jaramillo's technical support is greatly appreciated.

## References

[1] C. Misra, Industrial Alumina Chemicals, ACS Monograph 184, ACS, Washington, 1986.
[2] H. Knözinger, P. Ratnasamy, Cat. Rev.-Sci. Eng. 17 (1978) 31.
[3] K. Hellgardt, D. Chadwick, Ind. Eng. Chem. Res. 37 (1998) 405.
[4] K. Arata, Adv. Catal. 37 (1990) 165.
[5] T. Yamaguchi, Appl. Catal. 61 (1990) 1.
[6] D.A. Ward, E.I. Ko, J. Catal. 150 (1994) 18.
[7] D. Coster, A.L. Blumenfeld, J.J. Fripiat, J. Phys. Chem. 98 (1994) 6201.
[8] K. Tanabe, Appl. Catal. A 113 (1994) 147.
[9] E. Zhao, Y. Isaev, J.J. Fripiat, Catal. Lett. 60 (1999) 173.
[10] A. Krzywicki, M. Marczewski, J. Chem. Soc. Farad. Trans. I 76 (1980) 1311.
[11] G. Busca, G. Ramis, V. Lorenzelli, P.F. Rossi, A. La Ginestra, P. Patrono, Langmuir 5 (1989) 911.
[12] A. Stanislaus, M. Absi-Halabi, K. Al-Dolama, Appl. Catal. 39 (1988) 239.
[13] C. Morterra, G. Magnacca, P.P. De Maestri, J. Catal. 152 (1995) 384.
[14] A. Balankin, T. Lopez, R. Alexander-Katz, A. Cordova, O. Susarrey, R. Montiel, Langmuir 19 (2003) 3628.
[15] L.L. Hench, J.K. West, Chem. Rev. 90 (1990) 33.
[16] C.J. Brinker, G.W. Scherer, in: Sol–Gel Science: The Physics and Chemistry of Sol–Gel Processing, Academic, New York, 1990.
[17] D.M. Smith, R. Desphande, C.J. Brinker, W.L. Earl, B. Ewing, P.J. Davis, Catal. Today 14 (1992) 293.
[18] J. Sánchez-Valente, X. Bokhimi, F. Hernández, Langmuir 19 (2003) 3583.
[19] J. Sánchez-Valente, X. Bokhimi, J.A. Toledo, Appl. Catal. A 264 (2004) 175.
[20] X. Bokhimi, E. Lima, J. Valente, J. Phys. Chem. B 109 (2005) 22222.
[21] J. Sánchez-Valente, F. Hernández-Beltrán, M.L. Guzman-Castillo, J.J. Fripiat, X. Bokhimi, J. Mater. Res. 19 (2004) 1499.
[22] C.A. Fyfe, C.G. Gobbi, J.S. Hartman, J. Klinowski, J. Thomas, J. Phys. Chem. 86 (1982) 1247.
[23] E. Lippmaa, A. Samoson, M. Mägi, J. Am. Chem. Soc. 108 (1986) 1730.
[24] H.D. Morris, P.D. Ellis, J. Am. Chem. Soc. 111 (1989) 6045.
[25] C.S. Blackwell, R.L. Patton, J. Phys. Chem. 88 (1984) 6135.
[26] H. Benhamza, P. Barboux, A. Bouhaouss, F.A. Josien, J. Livage, J. Mater. Chem. 1 (1991) 681.
[27] A.I. Kozlov, M.C. Kung, W.M. Xue, H.H. Kung, Angew. Chem. Int. Ed. 42 (2003) 2415.